Journal of Membrane Science 572 (2019) 532–544

Contents lists available at ScienceDirect

Journal of Membrane Science

journal homepage: www.elsevier.com/locate/memsci

Biocatalytic PVDF composite hollow fiber membranes for CO_2 removal in gas-liquid membrane contactor

Yilin Xu[a,b], Yuqing Lin[b], Nick Guan Pin Chew[a,b], Chandresh Malde[c], Rong Wang[b,d,*]

[a] Interdisciplinary Graduate School, Nanyang Technological University, 50 Nanyang Avenue, Singapore 639798, Singapore
[b] Singapore Membrane Technology Centre, Nanyang Environment and Water Research Institute, Nanyang Technological University, 1 Cleantech Loop, Singapore 637141, Singapore
[c] Johnson Matthey Technology Centre, Reading RG4 9NH, United Kingdom
[d] School of Civil and Environmental Engineering, Nanyang Technological University, 50 Nanyang Avenue, Singapore 639798, Singapore

ARTICLE INFO

Keywords:
CO_2 removal
Gas-liquid membrane contactor
Biocatalytic membrane
Amine-functionalized membrane
Enzyme immobilization

ABSTRACT

A highly efficient biocatalytic carbonic anhydrase (CA)-polydopamine (PDA)/polyethylenimine (PEI)-polyvinylidene fluoride (PVDF) (referred to as CA-m-PVDF) composite membrane was fabricated for CO_2 conversion and capture in the gas-liquid membrane contactor (GLMC) process. The co-deposition of PDA/PEI with amino functional groups was employed to amine-functionalize a PVDF substrate as support for subsequent in-situ CA immobilization by cross-linking with glutaraldehyde. This enhances the enzyme stability and prolongs its lifespan, thus facilitates CO_2 hydration efficiency in the GLMC process. In this work, different immobilization CA protocols were compared based on the CA activity and activity recovery. For biocatalytic CA-m-PVDF membranes, the best activity of 498 U m^{-2} (membrane) and a corresponding activity recovery of 31.5% were achieved (m(5 h)-PVDF as support, 0.67 (v/v)% GLU as cross-linking agent, 600 μg mL^{-1} CA solution, pH 8.0, temperature at 25 °C, and 24 h reaction time). By using water as absorbent with a liquid velocity of 0.25 m s^{-1} in a bench-scale GLMC setup, a high-efficiency CO_2 absorption flux of 2.5×10^{-3} mol m^{-2} s^{-1} was obtained, which was ~165% higher than that of the non-biocatalytic m-PVDF membrane. The long-term stability test showed a good enzyme activity for CO_2 hydration capacity for the CA-m-PVDF membranes during 40 days of test duration. Overall, the results achieved in this work may provide promising insights into enzyme immobilization on polymeric supports for the development of high-efficiency biocatalytic membranes for CO_2 capture in GLMC applications.

1. Introduction

Gas-liquid membrane contactor (GLMC) is a gas-contacting configuration for CO_2 removal, which is achieved by flowing the gas/liquid fluid on both sides of a membrane in the concurrent or counter-current direction [1]. In this process, the hydrophobic microporous membrane acts as a non-selective interfacial barrier to separate the gas phase from liquid absorbents without dispersing one phase into the other. Gas diffuses from the bulk gas phase to the membrane surface before passing through the hydrophobic membrane pores. Subsequently, the gas transfers from gas-liquid interface to the bulk liquid followed by liquid phase absorption and/or chemical reaction [2]. GLMC has been proposed as a promising candidate for CO_2 capture over conventional absorption processes due to its main advantages of low energy consumption, small plant footprint, high operation flexibility, and facile scalability [1].

Currently, most of the traditional membranes applied in GLMC are typically fabricated with hydrophobic polymeric materials, such as polytetrafluoroethylene (PTFE), polypropylene (PP), polyethylene, polyvinylidene fluoride (PVDF), polysulfone (PSf), and polyetherimide [2–5]. The most commonly used liquid absorbents in CO_2 absorption processes are amine-based aqueous solutions, such as monoethanolamine (MEA), diethanolamine (DEA) and methyldiethanolamine (MDEA). These chemicals are highly corrosive and often consumed in large quantities. Polymeric membranes used in GLMC are easily swelled and degraded by amine aqueous solvents [6,7], which in turn can lead to membrane wetting and consequently significant CO_2 mass-transfer reduction. In addition, alkanoamine such as MEA could easily be degraded by oxygen, resulting in low CO_2 loading capacity [8]. The recovery of amine-based solvents or desorption of CO_2 needs to consume huge amounts of energy [9]. Therefore, it is desirable to use environmentally-benign solvents for CO_2 capture since it can decrease

* Corresponding author at: School of Civil and Environmental Engineering, Nanyang Technological University, 50 Nanyang Avenue, Singapore 639798, Singapore.
E-mail address: rwang@ntu.edu.sg (R. Wang).

https://doi.org/10.1016/j.memsci.2018.11.043
Received 19 August 2018; Received in revised form 22 October 2018; Accepted 18 November 2018
Available online 22 November 2018
0376-7388/

the consumption penalties of energy and investment for CO_2 capture in GLMC applications [10]. However, most benign solvents have much lower CO_2 loading capacity than that of the amine-based absorbents due to their lower CO_2 hydration kinetics. In order to address the rate-limiting problem of CO_2 hydration, a biocatalysis approach by using enzymes such as carbonic anhydrase (CA, E.C.4.2.1.1) as catalyst for CO_2 capture has received much attention [10,11].

The CA enzyme is a metalloenzyme involving zinc ion (Zn^{2+}), which has been widely studied due to its specific functionality of catalyzing reversible hydration CO_2 to bicarbonate ion (HCO_3^-) and proton [12]. Moreover, CA has a high turnover number of up to 10^6 mol CO_2 mol^{-1} CA s^{-1}, rendering it the fastest catalyst for CO_2 hydration [13]. The CA enzyme reaction of CO_2 hydration process can be expressed as follows (Eqs. (1)–(3)):

$$(Zn^{2+} — H_2O) \rightleftharpoons (Zn^{2+} — OH^-) + H^+ \quad (1)$$

$$(Zn^{2+} — OH^-) + CO_2 \rightleftharpoons (Zn^{2+} — HCO_3^-) \quad (2)$$

$$(Zn^{2+} — HCO_3^-) + H_2O \rightleftharpoons (Zn^{2+} — H_2O) + HCO_3^- \quad (3)$$

The catalytic CO_2 hydration equations are expected to be able to extrapolate to CO_2 absorption processes in GLMC as follows [12–16]: the active site of the CA enzyme refers to a Zn^{2+} coordinated by three histidine side-chains. A water molecule occupies the fourth coordination and contributes to the active site as well. Thus, the Zn^{2+} bound H_2O (Zn^{2+}—H_2O) acts as the origin of the donor and acceptor of the proton, from which a proton is released and transferred to the fourth histidine then to solvent, resulting in negatively charged Zn^{2+} bound hydroxide ion (Zn^{2+}—OH^-). The CO_2 diffuses from gas bulk through membrane phase and then reaches the biocatalytic layer. The CO_2 molecule attaches to (Zn^{2+}—OH^-) then converting to HCO_3^-, by nucleophilic attack of (Zn^{2+}—OH^-) on carbon atom of CO_2. Subsequently, the internal proton is transferred to form a Zn^{2+} bound HCO_3^- (Zn^{2+}—HCO_3^-), which is finally bounded with H_2O to form (Zn^{2+}—H_2O). Meanwhile, the HCO_3^- is released into the solvent. This speculation will be confirmed through a comprehensive set of characterization tests in this study.

In literature, enzymatic CO_2 capture has been widely studied for facilitating the CO_2 conversion in absorption, adsorption, and sequestration [17]. However, the drawbacks of free enzyme such as short lifetime and low stability under harsh operating conditions restrict its practical applications in CO_2 capture. To address these concerns, the preparation of biocatalytic materials based on enzyme immobilization has been proposed as a solution to improve the stability of the enzyme and thus increase the possibility of enzyme recovery and reuse [18–21].

Traditional enzyme immobilization can be achieved by chemical immobilization such as covalent bonding, cross-linking, and entrapment [10,11,15,18,21–23]. Chemical immobilization based on covalent bonds between the enzyme and the carrier is widely preferred as it provides much stronger bonding by increasing enzyme rigidity and avoiding leakage or dissociation [18]. The three-dimensional structure of enzyme could be more stable since the multipoint covalent bindings could prevent conformational changes induced by the environment. While the choice of immobilization strategies plays a crucial role in determining the biocatalytic material performance, various immobilization carriers with different chemical structure properties should also be taken into consideration. Carriers with functional groups such as amine, epoxy, carboxyl, sulfhydryl, hydroxyl, imidazole, indole, etc., could be involved in the binding [24,25]. Moreover, various supports such as nanoparticles [10,18,26], mesoporous silica SBA-15 [19,20], and Fe_3O_4 magnetic microspheres [21] have also been applied for CA immobilization after amine–, epoxy–, or carboxyl–functionalization. However, the immobilization of enzyme on pure polymeric membranes used for CO_2 capture has rarely been reported in literature. This could be due to the drawbacks of low enzyme activity recovery, poor enzyme stability, and membrane wetting. To address these issues, Yong et al. [11,27,28] proposed the layer-by-layer electrostatic adsorption method for preparing PP and PSf—polydimethylsiloxane based biocatalytic membranes layer-by-layer coated by mesoporous silica, polyethylenimine (PEI), polystyrene sulfonate, polyallylamine hydrochloride, and CA for CO_2 hydration in GLMC processes. Their experimental results suggested that the immobilization of CA on polymeric membranes can exhibit enhanced stability relative to their free states while maintaining their activity within the film for longer periods [28]. Iliuta et al. [16] investigated the CA based biocatalytic membrane in hollow fiber membrane bioreactors as a novel approach for CO_2 capture by using a series of simulations with different parameters of hollow fibers and different operation conditions in a multiscale steady-state model. This work proposed a promising concept for the biocatalytic CO_2 capture due to the advanced properties of low-cost and environment-friendly.

Different from reported works on CA immobilization, herein, we report the design and fabrication of biocatalytic CA-polydopamine (PDA)/PEI-PVDF (referred to as CA-m-PVDF) composite hollow fiber membranes via two-step co-deposition and cross-linking method for GLMC applications. The excellent adhesive feature of dopamine (DA)/PDA and rich amino functional groups of PEI were introduced to develop the PDA/PEI carrier for PVDF substrate functionalization, which is in favour of further enzyme immobilization [29,30]. The CA was subsequently in-situ immobilized on the amine-functionalized PVDF membrane via cross-linking with glutaraldehyde (GLU). The optimum conditions of preparing the biocatalytic composite membranes were investigated based on enzyme activity and activity recovery. Subsequently, different characterization tests were performed on the prepared biocatalytic hollow fiber membranes. Their CO_2 absorption performance was examined by using water and MEA as liquid absorbents in a bench-scale GLMC setup. Finally, the long-term stability of the biocatalytic membranes was examined. As shown in Fig. 1, the schematic illustration indicates the development of the biocatalytic composite hollow fiber membranes and their anticipated catalytic effects in the GLMC process.

2. Experimental

2.1. Materials and chemicals

PVDF hollow fiber membrane with an outer diameter of 1.5×10^{-3} m and an inner diameter of 0.8×10^{-3} m obtained from a commercial supplier [31] was used as substrate due to its desirable properties for GLMC applications such as high hydrophobicity of ~110°, suitable pore size of ~40 nm and pore size distribution, high porosity of ~85%, tough mechanical strength, and good thermal and chemical stabilities. Dopamine hydrochloride, PEI (Mw = 800), and tris(hydroxymethyl) aminomethane (Tris) were purchased from Sigma-Aldrich for the support preparation. CA from bovine erythrocytes (≥3500 W-A units/mg protein), GLU (50% in H_2O), 4-nitrophenyl acetate (p-NPA), and 4-Nitrophenol (p-NP) were purchased from Sigma-Aldrich for enzyme immobilization and assessment of the activity. Pure CO_2 (Singapore Oxygen Air Liquide Pte Ltd) as feed gas was applied for the GLMC experiments. Deionized water (DI water, produced by Milli-Q system, Millipore, USA) were used to prepare solutions and for CO_2 capture. MEA (≥99%, Sigma-Aldrich) was selected as a reference liquid absorbent for CO_2 absorption since it is a traditional and widely used absorbent in CO_2 absorption processes [32].

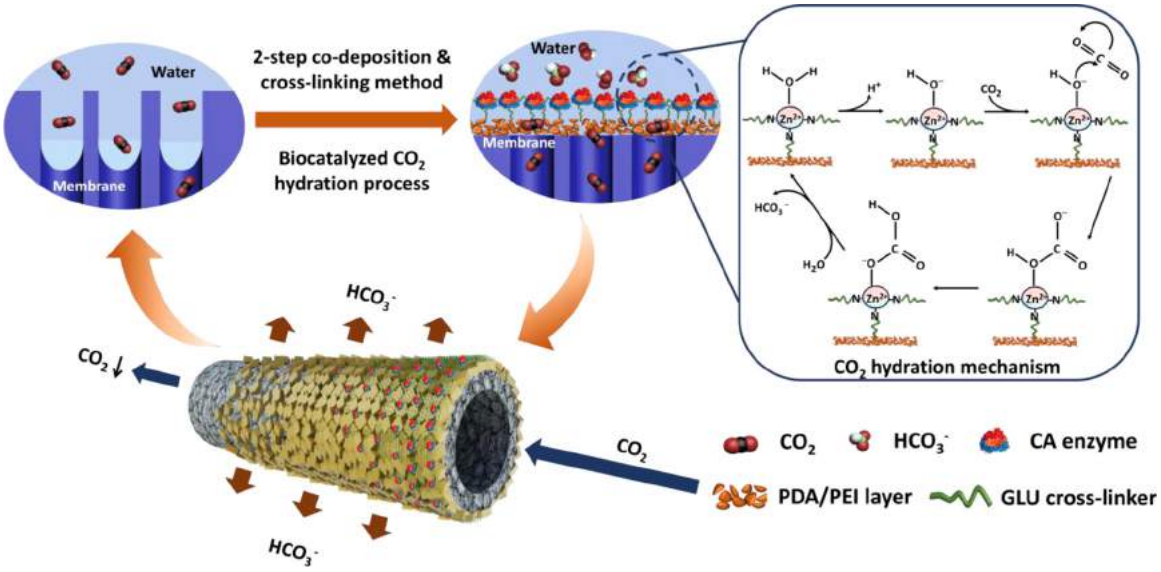

Fig. 1. Schematic illustration of the biocatalytic composite hollow fiber membrane and CO_2 absorption in GLMC process.

2.2. Preparation of an amine-functionalized membrane support

The commercial hydrophobic PVDF hollow fibers were used as substrates for PDA/PEI co-deposition on their shell side surface. Firstly, dopamine hydrochloride (2 mg mL^{-1}) and PEI (2 mg mL^{-1}) were dissolved in the Tris buffer solution (50 mM, pH = 8.5) [29,33]. Thereafter, pristine PVDF hollow fibers with their two sealed ends were immersed into the prepared deposition solution, shaking at 45 rpm for 3, 5, and 8 h (OM10E, OVAN, Spain). Finally, the treated hollow fibers were rinsed with DI water and then dried at 50 °C in an oven for 12 h. Hereon, the prepared amine-functionalized PVDF membranes are designated as the m-PVDF membranes.

2.3. Fabrication of biocatalytic composite hollow fiber membrane

The m-PVDF membranes were used as supports for enzyme immobilization. The hollow fibers (with two ends sealed with epoxy) were soaked in CA solutions with varied concentrations ranging from 100 to 1000 μg mL^{-1} in Tris buffer (50 mM) mixed with GLU with shaking at 40 rpm for certain times at different temperatures. After immobilization, the prepared biocatalytic hollow fibers were rinsed thoroughly with DI water and dried at room temperature for 24 h. Hereon, the developed biocatalytic PVDF composite hollow fiber membranes are referred to as CA(x)-m(y)-PVDF membranes, in which x and y refer to the concentration of CA solution and the coating time of PDA/PEI, respectively.

2.4. Enzyme activity assay and loading efficiency

The esterase activity of CA was determined by the rate of its catalyzing the hydrolysis of p-NPA to p-NP. Solutions of p-NP in water with concentrations ranging from 0.01 to 0.40 mM were prepared for drawing the p-NP standard curve, measured by a UV − vis spectrophotometry (UV-1800, SHIMADZU, Japan) at 384 nm. The p-NPA solution (3 mM) in water was prepared for the activity assays [27]. For the free CA enzyme, 0.1 mL of CA solution was mixed with 1.9 mL of Tris buffer (50 mM, pH 8) and 1 mL of p-NPA (3 mM). The mixture was stirred for 3 min and its absorbance was immediately measured. For the biocatalytic membranes, the hollow fiber sample was immersed in the assay solution (2 mL Tris buffer (50 mM, pH 8) and 1 mL p-NPA (3 mM)) and stirred for 3 min. After removing the hollow fiber sample, the absorbance of solution was quickly measured. In this work, one unit (U) of CA activity was defined by the amount of CA required to hydrolyze 1 μmol of p-NPA per minute at room temperature (25 °C). The units of the specific activities in the stock solution (free enzyme), on the biocatalytic membrane (immobilized enzyme), and remaining in the solution (un-immobilized enzyme) are U mg^{-1} (enzyme), U m^{-2} (membrane), and U mg^{-1} (enzyme), respectively.

The enzyme activity recovery and enzyme mass specific loading are generally used for quality and quantity evaluation of enzyme loading efficiency [10]. In this work, we used enzyme activity recovery to reflect the enzyme loading efficiency. The enzyme activity recovery is the proportion of the activity of the immobilized enzyme on the membrane surface in activity of the total free enzyme, which can be calculated by Eq.(4) [34]:

$$AR = \frac{A_{TE} - A_{UE}}{A_{TE}} \times 100\% \quad (4)$$

where AR is the enzyme activity recovery (%) based on activity loss in the enzyme solution, A_{TE} and A_{UE} are the activities (U mg^{-1} (enzyme)) of total free enzyme and un-immobilized enzyme in solution, respectively.

2.5. Membrane characterizations

The outer surface and cross-section morphologies and elemental composition of the samples of hollow fiber membranes were observed and detected by using a field emission scanning electron microscopy (FESEM, JSM-7600F JOEL, Japan) and an associated electron dispersive X-ray (EDX) spectroscopy, respectively, at an operation voltage of 5 kV, which were sputtered with a thin layer of platinum by a sputter coater (JEC3000FC, JEOL, Japan) prior to analysis. The membrane surface microstructures were examined by an atomic force microscopy (AFM, XE-100, Park System) in 5 μm × 5 μm scan size. The parameters of membrane surface roughness are represented by the roughness average (R_a) and the root-mean-squared roughness (R_q). The outer surface chemical functional groups of the prepared hollow fiber membranes were measured by a fourier-transform infrared spectroscopy—attenuated total reflectance (ATR-FTIR, IRPrestige-21, Shimadzu, Japan). The chemical composition of the outer and inner

surfaces of the hollow fibers were investigated by an X-ray photoelectron spectrometer (XPS, AXIS Supra, Kratos Analytical, UK) using monochromatic Al Kα excitation source at 1486.7 eV. The C 1s peak with the corrected energy at 284.5 eV was used as reference for spectra calibration. All XPS spectra for elements were analyzed by the CasaXPS software.

The average membrane pore size and pore size distribution were measured by a capillary flow porometer (CFP 1500A, PMI, Porous Material. Inc., USA) [35]. The dynamic water contact angle was examined by a tensiometer (DCAT11, Data physics, Germany) to evaluate the surface properties of the hollow fibers. A Zwick Roell Z0.5 universal testing machine was used for determining the mechanical properties of the hollow fiber membranes. Tensile modulus (E_t), tensile stress at break (σ_b) and strain at break (ε_b) were measured to indicate the mechanical stiffness and strength, and deformation of membrane under a given load.

Before characterization measurements, the prepared composite hollow fiber membranes underwent ultrasonic treatment at 25 kHz for 5 min in an ultrasonication bath (FB 15068, Fisher Scientific, USA) to remove any surface substances attached by van der Waals's force.

2.6. CO_2 absorption performance of biocatalytic membranes

A lab-scale module was prepared by sealing three pieces of hollow fibers in both ends of a glass tube with epoxy resin for preventing leakage, through which the effective length of hollow fiber was 4.4×10^{-2} m and the effective membrane area was about 6.4×10^{-4} m^2. Pure CO_2 as feed gas flowed in the lumen side of the hollow fibers, which was controlled and measured by a mass flow controller (Cole-Parmer®, USA) and a digital bubble meter (Bios-Dender 510L), respectively; the liquid absorbents of water and 1 M MEA (pH 11.9) were controlled by a digital peristaltic pump (MasterFlex® L/S, USA) and flowed over the shell side of the hollow fibers in a counter-current direction. For the leakage case, gas bubbles in the shell phase can be directly and clearly observed through the glass tube.

The CO_2 absorption flux can be calculated by the difference of the CO_2 inflow rate and outflow rate by Eq. (5):

$$J = \frac{P(Q_{in} - Q_{out})}{RTA_m} \times 10^3 \quad (5)$$

where J is the CO_2 absorption flux (mol m^{-2} s^{-1}) of the hollow fiber membrane, Q_{in} and Q_{out} are the volume flow rates (10^{-3} m^3 s^{-1}) of gas feed-in and feed-out, respectively, R the ideal gas constant of 0.083 bar L mol^{-1} K^{-1}, T the operating temperature of 298 K, A_m the membrane surface area (m^2), and P the operating pressure of 1 bar.

2.7. Long-term stability of the biocatalytic composite membrane

Several pieces of the biocatalytic CA(600)-m(5 h)-PVDF hollow fibers and free CA enzyme (600 μg mL^{-1}) were soaked and dissolved in the water (as absorbent for CO_2 capture), respectively, storing at the room temperature of 25 °C for 40 days to simulate the real-scenario of the contact process and evaluate their long-term stabilities. The activities of the biocatalytic membrane (immobilized CA) and free CA were examined by p-NPA method, periodically (see Section 2.4).

3. Results and discussion

3.1. Amine-functionalized PVDF hollow fiber membranes

In order to visually inspect on the morphologies and microstructures of the m-PVDF hollow fiber membranes with different PDA/PEI deposition durations, FESEM characterization and pore size analysis were carried out (Fig. 2). As shown in Fig. 2(a1) and (a2), the pristine PVDF was highly porous with a pore size of approx. 44 nm. After 3 h of coating, as shown in Fig. 2(b1) and (b2), it could be observed that PDA/PEI agglomerates were deposited on the PVDF substrate without fully covering its surface and forming a continuous layer, leading to a slight decrease in pore size (~36 nm). By further prolonging the coating time to 5 h, the agglomerates of PDA/PEI were uniformly deposited on the PVDF substrate and thoroughly covered the membrane pores, with a narrow pore size distribution and a smaller pore size of ~28 nm (shown in Fig. 2(c1) and (c2)). It was apparent that the pore size of the m-PVDF hollow fiber membrane decreases with increasing PDA/PEI coating time. After coating for 8 h, the PDA/PEI agglomerates further deposited on the surface of PVDF and generated a stratified structure due to the large agglomerates and the pore size of the m(8 h)-PVDF membrane decreased to ~16 nm (Fig. 2(d1) and (d2)). Similar observations can be found in studies conducted by Chew et al. [29,36] that the aggregation of PDA leads to the formation of hierarchical structures when the reaction time is prolonged. The co-deposition of PDA/PEI could have effectively covered most of the pores on the outer surface of the m-PVDF membrane and caused pore size reduction, which in turn could induce high membrane mass transfer resistance in the GLMC process, resulting in low CO_2 mass transfer.

The ATR-FTIR spectra verified the amine functionalization of the PVDF surface by co-deposition of PDA/PEI as shown in Fig. 3(a). The representative absorption peaks at 1339, 1474–1490, 1507–1577, 1610–1700 and 3000–3650 cm^{-1} could be attributed to the C-N stretching, aromatic C-C stretching of DA/PDA, amide II band (N-H bending (primary amines) and C-N stretching), amide I band (C=O stretching and C-N groups stretching), and N-H stretching (secondary amines) with O-H stretching, respectively [37]. Moreover, with increasing coating time, the density of amine functional groups was enhanced as reflected by the stronger representative absorption peaks. After coating with PDA/PEI for 8 h, the peaks of secondary amine together with hydroxyl functional groups were slightly stronger. This may be due to the more extensive cross-linking reactions between PDA and PEI thus consuming more primary amines. The DA in tris buffer solution could autoxidize to form different structures including dopamine quinone, leukochrome, aminochrome, 5,6-dihydroxyindole, and indole-5,6-quinone, and self-polymerize by covalently linking and/or intermolecular/supermolecular assembling various monomeric units to form PDA [38,39]. The primary amines of PEI could react with dopamine derivatives, dihydroxyindole, and/or indoledione to form Schiff bases and/or Michael-type adducts via Schiff base reaction and/or Michael addition, respectively [29,33,40]. Therefore, PEI cross-linked with PDA by covalent bonding and deposited on the PVDF substrate, thus reduced the physical self-assembling of PDA, resulting in a more stable amine-functionalized coating layer. The dynamic water contact angles of the pristine PVDF, m(3 h)-PVDF, m(5 h)-PVDF and m(8 h)-PVDF membranes are shown in Fig. 3(b), with the values of 110°, 64°, 61°, and 52°, respectively. It means that the hydrophobic PVDF substrate was altered to become hydrophilic after surface amine functionalization due to the hydrophilic properties of the PDA/PEI crosslinking layer.

Therefore, the m(5 h)-PVDF membranes with integrated PDA/PEI layer exhibited better surface microstructure with tighter pore size of 28 nm, narrower pore size distribution and less aggregations, and provided sufficient amine functional anchoring sites for the subsequent enzyme immobilization as discussed in Section 3.2.

3.2. Biocatalytic CA-m-PVDF hollow fiber membranes

3.2.1. Effects of amine-functionalized support, GLU and CA parameters on enzyme immobilization

In Fig. 4(a), different amine-functionalized support membranes were immersed in the pH 8, 200 μg mL^{-1} CA solution mixed with 0.67 (v/v)% GLU to further investigate the ideal amine-functionalized

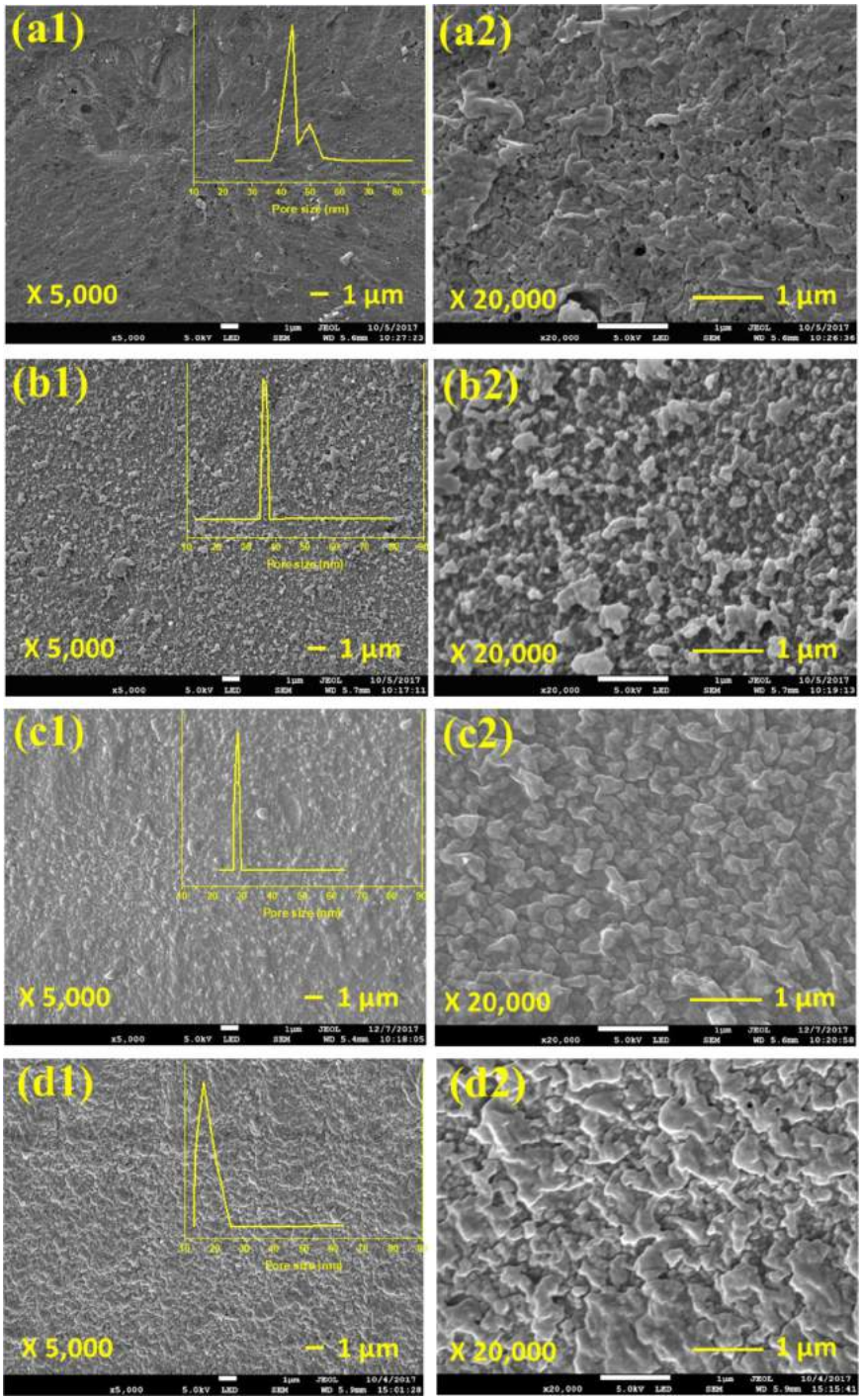

Fig. 2. FESEM images of the outer surface morphologies and pore size distributions of the PVDF (a1 and a2), ultrasonicated m(3 h)-PVDF (b1 and b2), m(5 h)-PVDF (c1 and c2), and m(8 h)-PVDF (d1 and d2) membranes.

membrane support for enzyme immobilization. The biocatalytic membrane with m(5 h)-PVDF support presented the best activity and enzyme activity recovery, since high density of the primary amine functional groups were provided for direct cross-linking with enzyme via covalent bonding [18]. On the other hand, the CA-m(8 h)-PVDF showed the relatively lowest enzyme activity and activity recovery. This could be explained by the fact that the longer chain of PDA/PEI enwrapped the enzyme and added steric hindrance between the support and the enzyme, thus resulting in enzyme activity reduction [22,41]. The deeper oxidative polymerization of DA/PDA and cross-linking with PEI resulted in less primary amine functional groups on the surface of the support, thus restricted the space of enzyme loading. Therefore, it has been further verified that the m(5 h)-PVDF composite membrane was an ideal polymeric support for enzyme immobilization.

As shown in Fig. 4(b), the m(5 h)-PVDF support membranes were immersed in the pH 8, 200 μg mL^{-1} CA solution mixed with 0.33–2.00 (v/v)% GLU to explore the optimal dosage of cross-linking agent for biocatalytic membrane development. The enzyme activity and activity

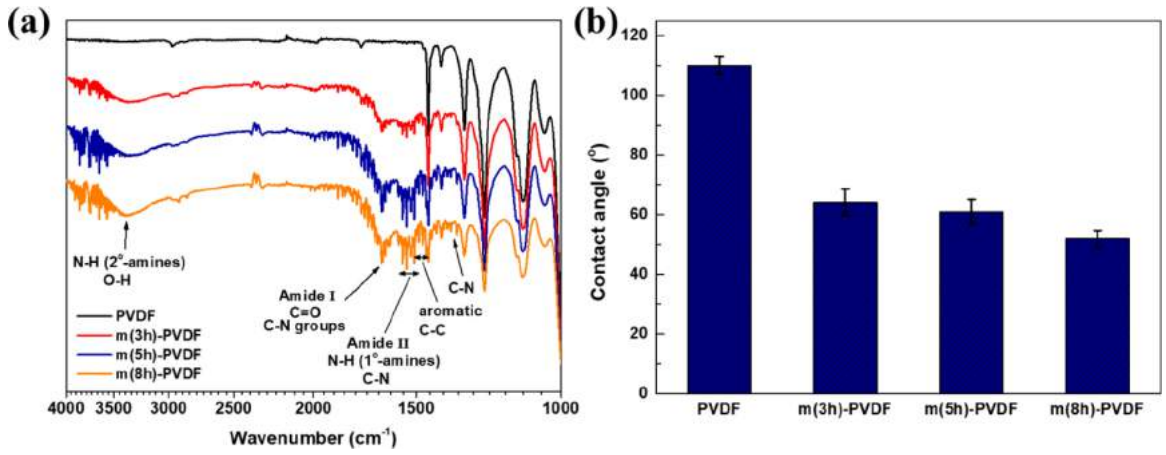

Fig. 3. ATR-FTIR spectra (a) and dynamic water contact angles (b) of the pristine PVDF, m(3 h)-PVDF, m(5 h)-PVDF and m(8 h)-PVDF membranes.

recovery exhibited an upward trend with increasing GLU concentration. Since GLU was introduced to bridge the membrane support and CA enzyme [19,24,42], there would be more active sites for enzyme immobilization. The immobilized enzyme on the membrane support likely reached saturation with GLU concentration of 0.67% based on activity and activity recovery. However, a significant decline was observed when the concentration of GLU exceeded beyond 1.33%. Since any excess aldehyde groups of GLU would react with the enzyme, this might lead to a structural change in the enzyme and a subsequent decrease of activity.

In Fig. 4(c), the m(5 h)-PVDF support membranes were soaked in the pH 8 CA solution with different concentrations of 100–1000 μg mL^{-1} mixed with 0.67 (v/v)% GLU, to explore the optimal concentration of CA for achieving the best enzyme activity of the biocatalytic membrane. The activity of biocatalytic membrane increased with increasing concentration of CA solution for immobilization [18], where the highest activity was achieved by 600 μg mL^{-1} CA concentration. However, by continuously increasing the CA concentration, enzymes might overcrowd on the support and aggravate the steric hindrance, thus resulting in the deterioration of enzyme activity on the biocatalytic membrane. In contrast, the enzyme activity recovery on membrane surface decreased with increasing enzyme concentration, which was in accordance with other reported works [34,43,44]. This is because a higher offered CA concentration led to a lower efficiency of enzyme immobilization, even though the amount of immobilized enzyme would be increased [44,45]. The enzyme loading would almost reach the saturation level for the membrane support with a certain density of amine functional groups, when offered around 400–600 μg mL^{-1} CA for immobilization.

3.2.2. Effects of pH, temperature, and cross-linking time on enzyme immobilization

As shown in Fig. 5(a), the effect of immobilization pH varying from 6.0 to 9.0 on enzyme activity and activity recovery was investigated because CA generally prefers a weak alkaline environment to maintain its activity. The CA activity as well as enzyme activity recovery increased with increasing pH value from 6.0 to 8.0, and afterwards decreased by continuing increasing the pH value to 9.0. When at high pH value conditions, the electrification state of the free CA and magnetic microspheres would be transformed, thus affecting the enzyme activity and immobilization procedure [20]. Therefore, the optimum pH for enzyme immobilization was 8.0.

The effect of temperature on relative enzyme activity and activity recovery on membrane support is shown in Fig. 5(b). The enzyme activity at 20 °C condition was the lowest, due to low temperature resulting in slower reaction rate. When the temperature increased to 25 °C, the activity and activity recovery both achieved the highest values, then decreased along with temperature, since enzymes are highly sensitive to high temperature.

As shown in Fig. 5(c), the effect of immobilization time varying from 6 h to 36 h on enzyme activity and activity recovery was explored. With an increase of reaction time, both CA activity and its recovery of the immobilized enzyme on the polymeric support increased. The best relative activity and activity recovery for CA immobilization on membrane support were achieved with a reaction time of 24 h, while the relative enzyme activity decreased by prolonging the immobilization time to longer than 24 h. This is likely due to the active site of the membrane support reaching the equilibrium status at 24 h. By continuously prolonging the immobilization time to 36 h, the enzyme could be multipoint cross-linked by GLU and the conformation of the enzyme might be influenced [18], thus resulting in enzyme activity degradation.

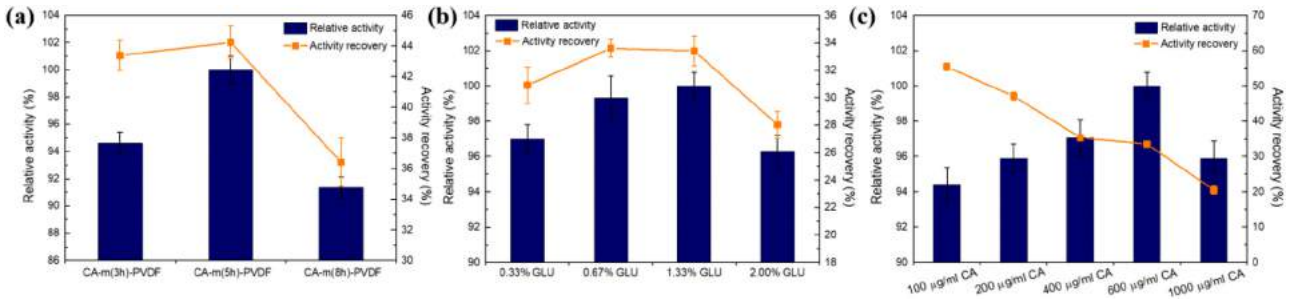

Fig. 4. Relative activity and enzyme activity recovery for biocatalytic CA-m-PVDF membranes at different (a) m-PVDF supports (0.67% GLU; 200 μg mL^{-1} CA; pH 8.0; 25 °C; 24 h for enzyme immobilization), (b) concentrations of GLU (m(5 h)-PVDF; 200 μg mL^{-1} CA; pH 8.0; 25 °C; 24 h for enzyme immobilization), (c) concentrations of CA (m(5 h)-PVDF; 0.67% GLU; pH 8.0; 25 °C; 24 h for enzyme immobilization).

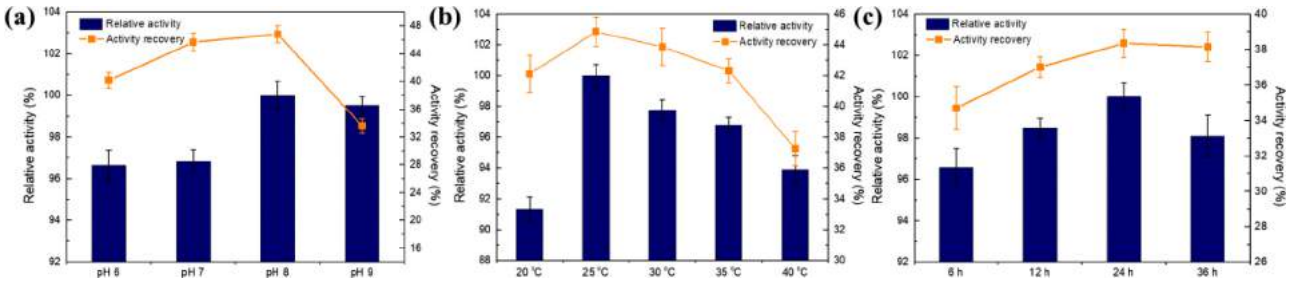

Fig. 5. Relative activity and enzyme activity recovery for biocatalytic CA-m-PVDF membranes under different (a) pH values (m(5 h)-PVDF; 0.67% GLU; 200 μg mL^{-1} CA; 25 °C; 24 h), (b) temperatures (m(5 h)-PVDF; 0.67% GLU; 200 μg mL^{-1} CA; pH 8.0; 24 h), (c) reaction times (m(5 h)-PVDF; 0.67% GLU; 200 μg mL^{-1} CA; pH 8.0; 25 °C) for enzyme immobilization.

Therefore, according to the measurements of activity and activity recovery of the prepared biocatalytic membranes based on various immobilization conditions, the biocatalytic CA(600)-m(5 h)-PVDF composite hollow fiber membranes cross-linked by 0.67% GLU under the immobilization environments of pH 8.0 at 25 °C for 24 h could achieve the best activity of 498 U m^{-2} (membrane) and the corresponding activity recovery of 31.5%, for the following membrane characterizations as well as CO_2 capture performance that will be discussed in Sections 3.3 and 3.4. The activity of the biocatalytic CA(600)-m(5 h)-PVDF composite hollow fiber membranes was comparable to a previously reported biocatalytic membrane [10].

3.3. Membrane characterizations

3.3.1. Morphologies and physical properties of biocatalytic CA-m-PVDF composite hollow fiber membranes

Fig. 6 shows the shell surface and cross-section morphologies of the biocatalytic CA(600)-m(5 h)-PVDF composite hollow fiber membrane after ultrasonication. It could be observed that the biocatalytic layer remained integrated, implying a robust modification layer under harsh conditions. By comparison with the m(5 h)-PVDF membrane, as shown in Fig. 2(c1) and (c2), it could be observed that the microstructures in terms of the surface morphologies and pore size/pore size distributions of the biocatalytic CA(600)-m(5 h)-PVDF composite membrane were not significantly changed after the CA immobilization. However, for the m(5 h)-PVDF membrane, the deposited PDA/PEI agglomerates on the PVDF substrate constructed a hierarchical geometry structure with a higher roughness, as presented in Table 1. In contrast, after the CA immobilization, the surface roughness of CA(600)-m(5 h)-PVDF membrane slightly decreased, since the CA were filled in the low-lying "valleys" during the immobilization process, with reference to Fig. A1. As shown in Fig. 6(c) and (d), the biocatalytic CA-PDA/PEI layer, with a thickness of around 0.25 μm, was deposited on the PVDF substrate with sponge-like structure.

Fig. 7 shows the EDX characterization results of the shell surface and cross-section of the biocatalytic CA(600)-m(5 h)-PVDF composite hollow fiber membranes. The elemental distributions of N, O, and Zn were selected as the distribution indicator for amine and amide groups of PDA, PEI, and CA. In Fig. 7(a1)–(a5), we can observe that the N, O, and Zn elements were evenly and thoroughly distributed on the membrane surface, verifying the formation of a continuous biocatalytic layer on the PVDF substrate surface. Fig. 7(b1)–(b5) presents the EDX mappings of membrane cross-section where the N and O elements were mostly deposited on the outer surface of the prepared hollow fiber

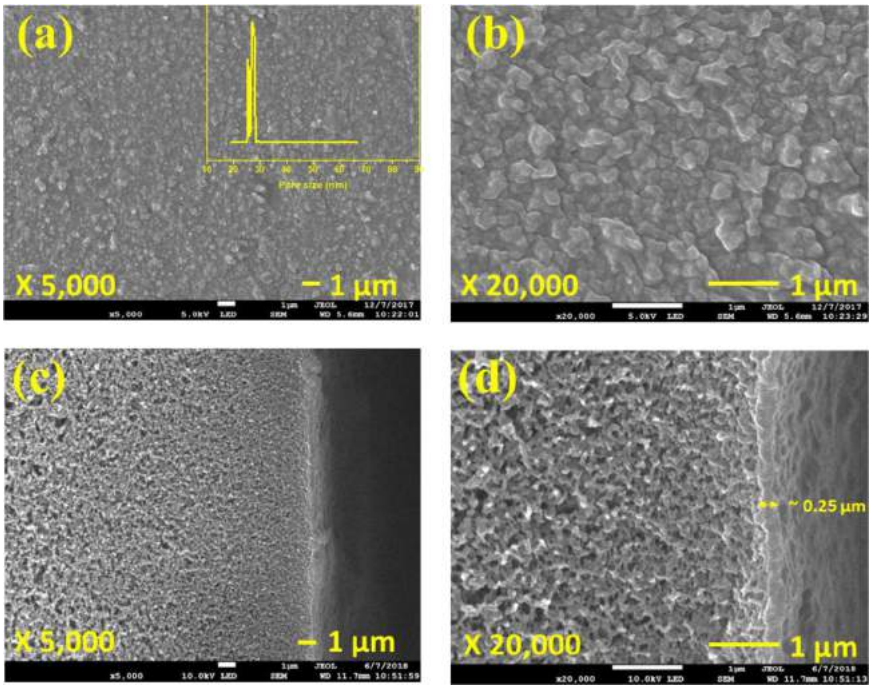

Fig. 6. FESEM images of the outer surface (a and b) and cross-section (c and d), and pore size distributions (a) of the ultrasonicated CA(600)-m(5 h)-PVDF membranes.

Table 1
Surface roughness parameters, mechanical properties and contact angles of the PVDF, m-PVDF and CA-m-PVDF hollow fiber membranes.

Membrane	Roughness		Mechanical properties			Dynamic
	R_a (nm)	R_q (nm)	E_t (MPa)	σ_b (MPa)	ε_b (%)	contact angle (°)
PVDF	10.67 ± 1.40	8.26 ± 1.12	26.2 ± 2.4	2.00 ± 0.09	97.4 ± 4.1	110.0 ± 2.9
m(5 h)-PVDF	26.80 ± 0.94	33.35 ± 1.41	31.5 ± 2.8	2.27 ± 0.05	80.9 ± 4.8	60.9 ± 4.2
CA(600)-m(5 h)-PVDF	23.67 ± 1.08	29.83 ± 1.32	28.4 ± 2.1	2.25 ± 0.11	85.2 ± 4.6	59.7 ± 2.2

membrane while small traces could be detected in the bulk of the PVDF substrate. This might be ascribed to the image noise of the N and O elements, or PDA/PEI solution penetrated into the PVDF substrate pores via the amine functionalization process. However, the Zn mapping image exhibited weak signal intensity due to the lower content of Zn^{2+} in the immobilized CA molecules, since there is only one Zn^{2+} coordinated in one CA molecule theoretically. Therefore, it is hard to obtain the clear Zn elemental distribution via EDX scanning, especially for the cross-section EDX mapping of Zn element. Consequently, we examined the CA modification layer by tracing the elements of N, O, and Zn together, rather than tracing only one element of Zn. Moreover, the successful CA immobilization could be also ascertained by the enzyme activity assay and the CO_2 conversion performance in GLMC application.

The mechanical properties and surface hydrophilicity were evaluated for the CA(600)-m(5 h)-PVDF, m(5 h)-PVDF, and PVDF membranes, as shown in Table 1. The m(5 h)-PVDF and CA(600)-m(5 h)-PVDF composite membranes presented slightly higher rigidity ascribing to the fragile nature of the PDA/PEI [46] and rigid structure of the immobilized enzyme [18]. The shell surface of the hydrophobic PVDF membrane was tuned to be hydrophilic after two steps of surface modification, since the amine-, amide-, and hydroxyl-functional groups of PDA/PEI and immobilized CA imparted hydrophilic properties to the m(5 h)-PVDF and CA(600)-m(5 h)-PVDF membrane surfaces.

3.3.2. Chemical composition of biocatalytic CA-m-PVDF composite hollow fiber membranes

The ATR-FTIR spectra of PVDF, m(5 h)-PVDF and CA(600)-m(5 h)-PVDF hollow fiber membranes to verify the two-step cross-linking procedure for immobilizing CA on the amine-functionalized PVDF membrane surface are shown in Fig. 8. It could be observed that after immobilizing CA on the m(5 h)-PVDF membrane surface, the absorption peaks of C-N, aromatic C-C, N-H (primary amines), and C=O were slightly weaker, while the peaks of N-H (secondary amines) with O-H were stronger. This is due to CA immobilized on the PDA/PEI layer by cross-linking with GLU through covalent bonding, which consumed the primary amine or amino groups of PDA/PEI and CA enzyme, resulting in denser secondary amine groups and less related functional groups of PDA/PEI on the membrane shell surface.

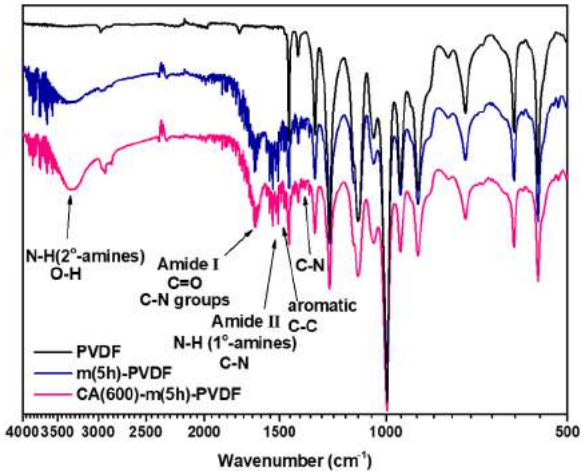

Fig. 8. ATR-FTIR spectra of the shell surfaces of the PVDF, m(5 h)-PVDF and biocatalytic CA(600)-m(5 h)-PVDF membranes.

Table 2
Elemental composition (%) of the outer/inner surfaces of the PVDF, m(5 h)-PVDF and CA(600)-m(5 h)-PVDF membranes.

	C 1s (%)	F 1s (%)	O 1s (%)	N 1s (%)	Cl 2p (%)
Outer surface					
PVDF	56.5	28.3	2.0	–	13.2
m(5 h)-PVDF	71.6	3.1	15.5	9.8	–
CA(600)-m(5 h)-PVDF	74.5	0.3	17.5	5.8	1.9
Inner surface					
PVDF	52.8	31.9	1.0	–	14.3
m(5 h)-PVDF	54.5	30.3	0.6	–	14.6
CA(600)-m(5 h)-PVDF	51.8	32.9	1.6	–	13.7

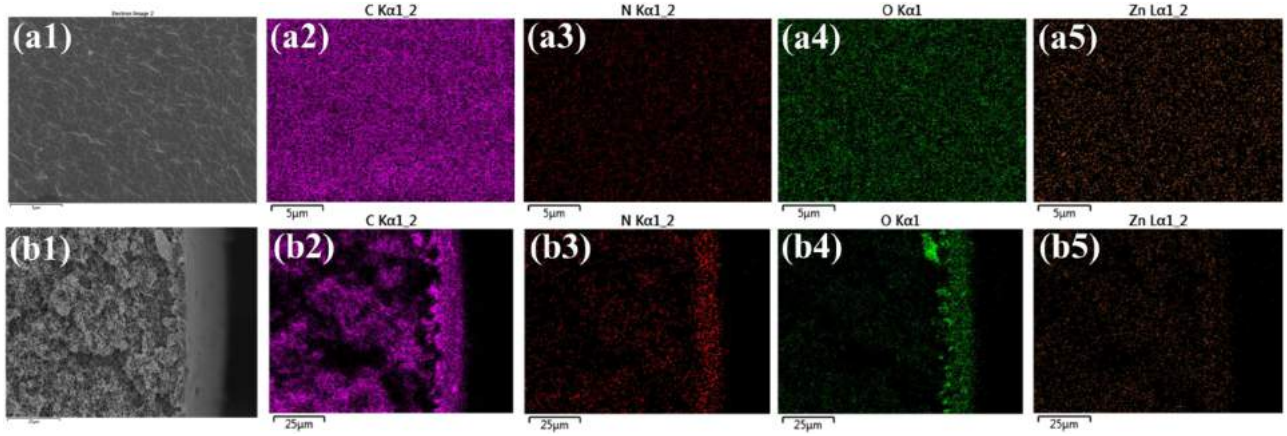

Fig. 7. (a1 and b1) the outer surface and cross-section images of biocatalytic CA(600)-m(5 h)-PVDF composite membrane, and EDX mappings for (a2 and b2) C, (a3 and b3) N, (a4 and b4) O, (a5 and b5) Zn elements.

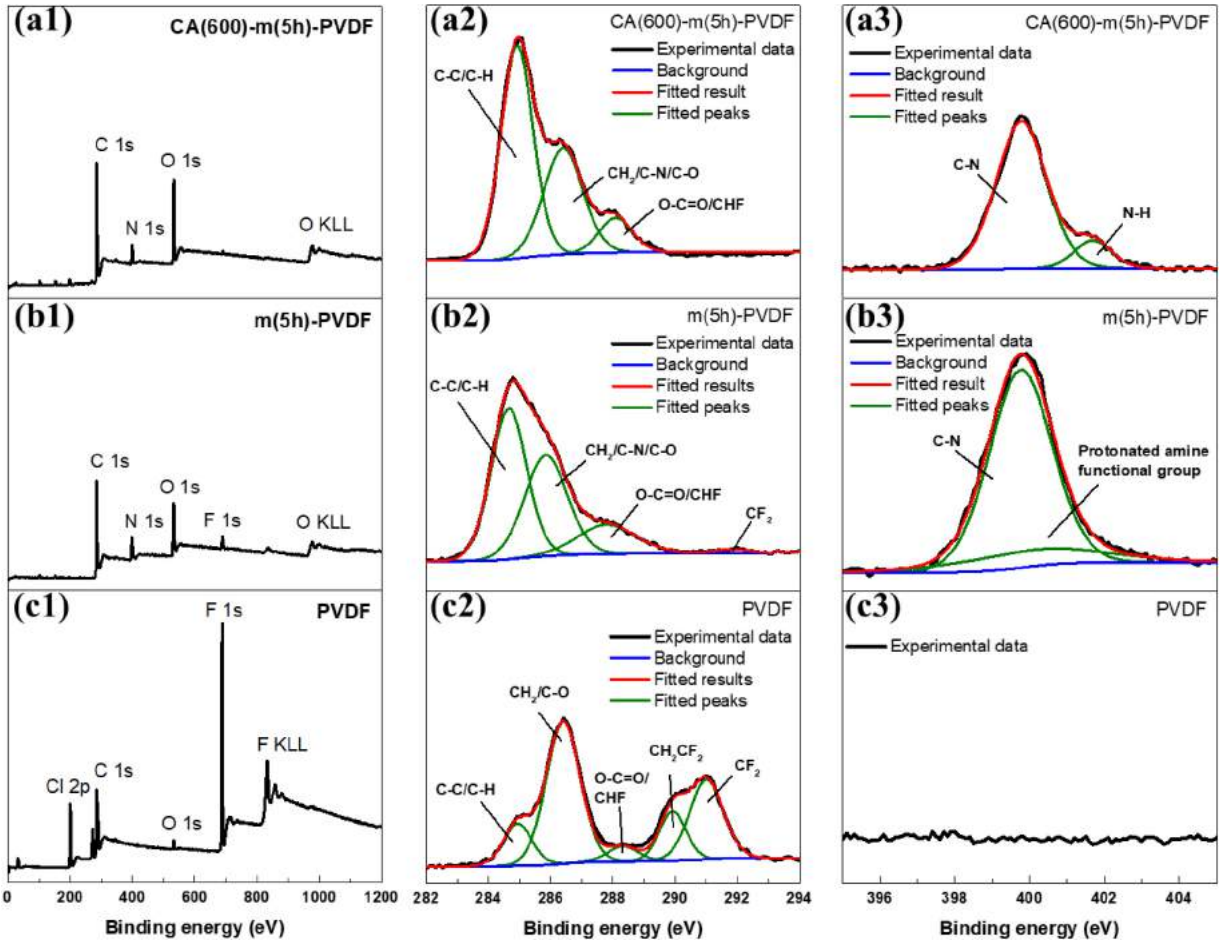

Fig. 9. (a1, b1 and c1) XPS survey scan spectra, and high-resolution C 1s (a2, b2 and c2), N 1s (a3, b3 and c3) XPS spectra of the outer surfaces of the CA(600)-m(5 h)-PVDF, m(5 h)-PVDF and PVDF membranes.

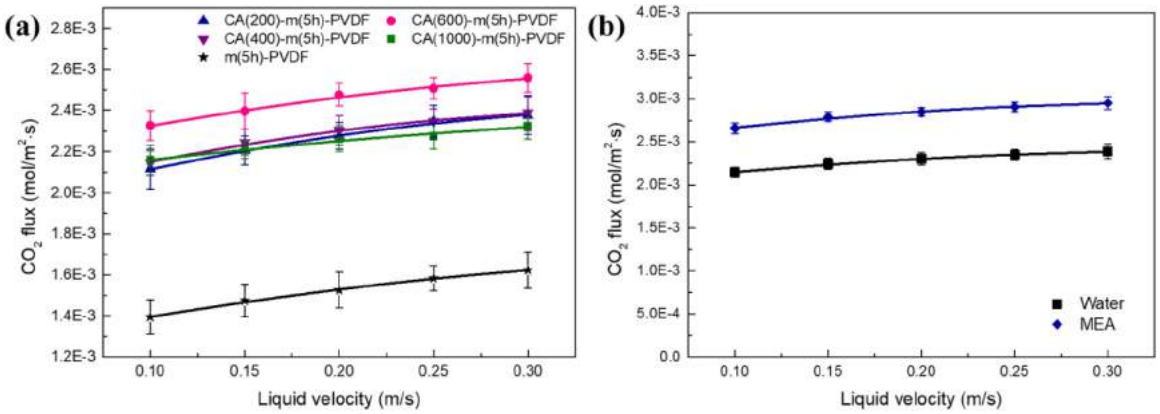

Fig. 10. CO_2 absorption flux of biocatalytic CA-m-PVDF composite membranes with different (a) CA loading concentrations (200–1000 μg mL^{-1}) and (b) liquid absorbents (water and 1 M MEA).

XPS analysis was carried out to further investigate the elemental composition and chemical bonding of the PDA/PEI layer and the immobilized CA layer. As listed in Table 2, the inner surface elemental compositions of the PVDF substrate, m(5 h)-PVDF, and CA(600)-m(5 h)-PVDF membranes were similar, which indicates that the PDA/PEI and CA layers did not penetrate the bulk of the PVDF substrate, thus maintaining its hydrophobicity for resisting pore wetting. However, the elemental compositions of outer surface for obtained membrane are different. The peaks of the F 1s and Cl 2p were significantly weakened and eventually disappeared along with grafting PDA/PEI and then immobilizing CA on the shell surface of the PVDF substrate, while the peaks of N 1s and O 1s strengthened accordingly, as shown in Fig. 9(a–c1). It implies that the CA immobilized on PDA/PEI layer completely covered the pristine PVDF membrane surface. The

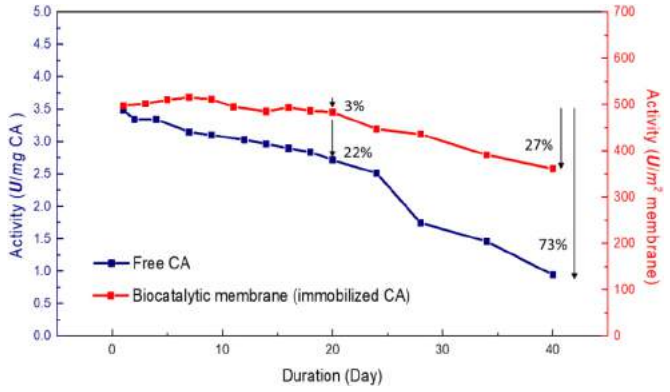

Fig. 11. The long-term activities of biocatalytic membrane and free CA enzyme in absorbent of water over 40 days storage.

deconvolution of C 1s spectra (Fig. 9(a–c2))were curve-fitted to five components with binding energies of 284.8 eV, 286.2 eV, 288.1 eV, 289.9 eV, 291.2 eV, respectively, which were assigned to the C-C/C-H, CH_2/C-N/C-O, O-C=O/CHF, CH_2CF_2, and CF_2 bonds, respectively [29,46,47]. And the deconvolution of N 1s spectra (Fig. 9(a–c3)) were peak-fitted with two or three peak components with binding energies of 399.8 eV, 400.1 eV and 401.7 eV for the C-N band, the protonated amine-functional groups, and N-H bond, respectively. Compared with pristine PVDF substrate, the peak of C-C/C-H for the m(5 h)-PVDF membrane was significantly enhanced, on the contrary, the peak of CH_2CF_2 was disappeared and the peak of CF_2 was weaken to slight level. Moreover, the new C-N peak as well as the protonated amine-functional group peak were generated, which could be ascribed to the co-deposition of PDA/PEI aggregates. For the CA(600)-m(5 h)-PVDF composite membranes, the peaks of C-C/C-H and CH_2/C-O were further increased, which contributed to the CA cross-linked with GLU immobilized on the PDA/PEI layer, while the C-N peak became slightly weakened accordingly.

According to the above XPS spectra results, we attempted to propose the mechanisms of immobilization CA on the PDA/PEI support layer as follows: the PVDF was pre-activated by amine groups after co-depositing the PDA/PEI aggregates on the PVDF surface as carriers for enzyme immobilization [48]. The PDA/PEI layer provided abundant primary amine groups and multiple binding sites for immobilizing the enzyme via GLU as cross-linker [22,25]. The GLU molecules multi-pointed covalently reacted with the three-dimensional structure of CA with α-amino groups of histidine residues, as well as reacted with the amino groups of the m(5 h)-PVDF support, resulting in Schiff's base formation, then establishing intermolecular cross-linkages. The formation of the immobilized CA became more rigid, which prevented conformational changes caused by temperature, pH, solvents, etc., intermolecular aggregation, and autolysis [18,49].

3.4. CO_2 absorption performance of the biocatalytic composite membrane in GLMC

In order to examine the performance of biocatalytic CA-m-PVDF composite membranes with different concentrations of CA enzyme, the CO_2 absorption flux performance of the CA(200)-, CA(400)-, CA(600)-, and CA(1000)-m(5 h)-PVDF composite hollow fiber membranes and the non-biocatalytic m(5 h)-PVDF membrane as a comparison were measured. We can observe from Fig. 10 (a) that the CO_2 fluxes of the developed biocatalytic composite membranes were significantly higher than that of the non-biocatalytic m(5 h)-PVDF membrane. Since the biocatalytic membrane offered sufficient long chained PDA/PEI molecules that provided adequate space between the membrane and the enzyme, it leads to a good enzyme conformational flexibility and

Table 3
Comparison of CO_2 absorption flux of the various microporous hollow fiber membranes in GLMC.

Membrane substrate	Modification layer	Fiber OD/ID (mm)	Pore size (nm)	Lumen side	Feed gas	Absorbent	Liquid velocity (m s^{-1})	CO_2 flux (10^{-3} mol m^{-2} s^{-1})	Reference
PVDF	CA-PDA/PEI	1.53/0.85	26	Gas	Pure CO_2	Water	0.25	2.5	Current work
PVDF	–	0.8/0.55	55	Gas	Pure CO_2	Water	0.25	0.2	[52], 2013
PVDF-*co*-hexafluoropropylene	Fluorolink S10 & tetraethoxysilane	–	25	Gas	Pure CO_2	Water	0.25	0.6	[53], 2011
Polyetherimide	Fluorinated SiO_2	1.1/0.8	40	Gas	Pure CO_2	Water	0.25	1.3	[54], 2013
Poly(amieimide)	Octadecylamine	1.44/1.1	–	Gas	Pure CO_2	Water	0.25	1.8	[55], 2012
PSf	–	1.0/0.5	11	Liquid	Pure CO_2	Water	0.3	0.8	[56], 2010
PP	–	0.3/0.22	40	Liquid	20% CO_2	Water	0.25	0.2	[3], 2006
PP	Fluorinated TiO_2	2.7/1.8	200	Gas	20.4% CO_2	0.1 M buffer with 200 μg mL^{-1} CA[a]	405 mL·min^{-1}	0.2	[26], 2016
PVDF	–	1.0/0.65	200	Liquid	Pure CO_2	2 M MEA	2.1	2.6	[5], 2007
PTFE	–	2.44/1.83	30–80	Liquid	Pure CO_2	30 wt% MEA	28 mL·min^{-1}	1.1	[51], 2014
Al_2O_3	Fluorinated ZrO_2	12.0/8.0	200	Liquid	12.5% CO_2	5 wt% MEA	10 mL·min^{-1}	1.3	[57], 2015
PVDF	Fluorinated TiO_2	1.46/0.76	25	Gas	Pure CO_2	1 M MEA	0.25	10.9	[58], 2018
PVDF	Fluorinated TiO_2-SiO_2	1.2/0.7	25	Gas	40% CO_2	1 M MEA	0.25	3.2	[47], 2018

[a] pH 10, 0.1 M sodium carbonate/sodium bicarbonate buffer with 200 μg mL^{-1} immobilized CA.

realizes a high activity for CO_2 conversion [25]. While CO_2 absorption in water is physical process, the presence of the CA with active site of Zn^{2+} coordinated by three histidine side-chains can significantly enhance the kinetics of CO_2 conversion by catalyzing CO_2 hydration to HCO_3^- and H^+ [12–16]. Even though the biocatalytic and non-biocatalytic membranes could be partially wetted induced by their hydrophilicity, the significantly accelerated CO_2 conversion by the superb catalysis of the immobilized CA on membrane surface could circumvent the negative impact of membrane wetting [16]. However, the CO_2 fluxes of the biocatalytic membranes showed gently rising trends with liquid velocities from 0.1 to 0.3 m s^{-1}. It may be ascribed to the fact that the CO_2 removal efficiency was mainly controlled by the immobilized CA catalyzing CO_2 hydration on the gas-liquid boundary rather than the refresh rate of the liquid absorbent.

It can be observed that the CO_2 fluxes of the biocatalytic composite membranes with different CA loadings presented positive correlation with the enzyme activities, thus further verified the enhancement of CO_2 mass transfer by the immobilized CA in GLMC process. In particular, the CA(600)-m(5 h)-PVDF composite membrane with the highest activity presented the highest CO_2 absorption performance with flux value of 2.6×10^{-3} mol·m^{-2}·s^{-1} at water velocity of 0.3 m s^{-1}. The other biocatalytic membranes offered with 200, 400, 1000 μg mL^{-1} CA all exhibited similar CO_2 absorption performance due to their lower expressed enzyme activities at almost the same level (see Section 3.2.1).

In Fig. 10(b), the CO_2 absorption performances of the biocatalytic composite hollow fiber membranes were also examined using liquid absorbents of 1 M MEA in order to verify the feasibility of biocatalysis for CO_2 conversion using traditional amine-based absorbents. The CO_2 flux of the biocatalytic membrane using MEA presented only a 7% increment over that of water, which is much lower than the previously reported result (~ 200% increment) [5]. This is due to the fact that the activity of immobilized enzyme could be compromised in extremely alkaline environment. Khameneh et al. [50] and Lv et al. [20] discovered that the activity of the immobilized CA could be reduced by up to 40–80% at pH 12. Moreover, due to the hydrophilic nature of the biocatalytic layer, the top layer of the composite membrane actually was partially wetted thus resulting in extra membrane resistance for CO_2 mass transfer, which was in good agreement with a study conducted by Iliuta et al. [16]. Therefore, low-efficiency of biocatalysis for CO_2 conversion in the extremely alkaline environment and induced high membrane resistance would severely restrict the performance of MEA for CO_2 absorption, resulting in an inadequacy in importing amine aqueous absorbent to the biocatalytic membrane in the GLMC process. Just using water as the absorbent for the prepared biocatalytic membrane could achieve a reasonable CO_2 removal performance. Coupled with the benefits of low-cost and environment-friendly, water can be an attractive option for CO_2 removal in GLMC processes.

3.5. Long-term stability of the biocatalytic composite membrane

The activities of two forms of enzyme—immobilized CA on membrane support and free CA in water (as catalyzers immobilized on the gas-liquid interface and dissolved in the liquid absorbent phase, respectively) were investigated at 25 °C for 40 days to evaluate their long-term stabilities, as shown in Fig. 11. The activity of biocatalytic CA(600)-m(5 h)-PVDF composite hollow fiber membrane maintained a relative high value of 484 U m^{-2} of membrane with merely 3% reduction from the initial value of 498 U m^{-2} of membrane over a 20-day period. After 40 days, the activity of biocatalytic membrane retained 73% of its initial activity. In comparison, the activity of free CA enzyme continuously declined during the 40-day observation. The activity showed a 22% reduction, decreasing from 3.5 to 2.7 U mg^{-1} of enzyme after 20 days, and then sharply decreased to 0.9 U mg^{-1} of enzyme, losing 73% of its initial activity after 40 days. The immobilized CA on membrane surface presented a more robust long-term stability compared with free enzyme in solution, thus further validating the appealing features of the proposed biocatalytic composite membrane for CO_2 absorption in GLMC application. This could be ascribed that the formation of multiple covalent bonds between the enzyme, cross-linker, and amine-functionalized membrane support reduced the conformational flexibility and thermal vibration, resulting in the avoidance of enzyme unfolding and denaturation and enhancing the stability of CA [21,25].

Therefore, we can conclude that the prepared biocatalytic CA(600)-m(5 h)-PVDF composite membrane achieved reasonable CO_2 removal performance as well as long-term stability, which provides useful insights into a potential biocatalytic composite hollow fiber membrane for CO_2 capture in the GLMC process.

3.6. CO_2 absorption performance comparison with various membranes for GLMC

The CO_2 absorption performance of various microporous hollow fiber membranes in GLMC processes is summarized in Table 3. There have been very few research works introducing enzyme in GLMC processes [11,26]. Compared with other works using traditional hydrophobic polymeric hollow fibers and water as liquid absorbent, the prepared biocatalytic CA(600)-m(5 h)-PVDF composite hollow fiber membrane developed in this work exhibited strongly competitive CO_2 removal performance, with a high flux value of 2.5×10^{-3} mol m^{-2} s^{-1} at liquid velocity of 0.25 m s^{-1}. It is worth noting that the biocatalytic CA-m-PVDF composite membranes using pure CO_2 as feed gas and water as absorbent could be comparable with some PVDF and PTFE membranes applied with higher concentrations (2 M and 30 wt% (≈ 4.9 M)) of MEA absorbents [5,51]. This can be ascribed to the high-efficiency CO_2 hydration on immobilized CA enzyme catalysis being beneficial to CO_2 conversion in GLMC processes [11,13].

4. Conclusions

A two-step co-deposition and cross-linking method was proposed to prepare biocatalytic CA-m-PVDF composite hollow fiber membranes for CO_2 removal in the GLMC process. Different immobilization CA protocols were compared based on CA activity and loading efficiency (activity recovery). For the GLMC application, the best biocatalytic CA-m-PVDF composite membranes exhibited high CO_2 removal flux with a value of 2.5×10^{-3} mol m^{-2} s^{-1}, by using water as absorbent with a liquid velocity of 0.25 m s^{-1}, increasing ~160% higher than that of the pristine m-PVDF membrane without CA biocatalysis. A robust long-term activity of the biocatalytic CA-m-PVDF composite membranes was also realized in a 40-day observation. This work provides an insight into enzyme immobilization on polymeric supports for developing high-efficiency biocatalytic membranes for CO_2 capture in GLMC applications, which is cost effective and environmentally friendly.

Acknowledgements

This work was funded by the Johnson Matthey Public Limited Company, UK. We also acknowledge funding support from the Singapore Economic Development Board, Singapore to the Singapore Membrane Technology Centre.

Appendix A. AFM images of the PVDF substrate, m-PVDF and CA-m-PVDF composite membranes

See Fig. A1.

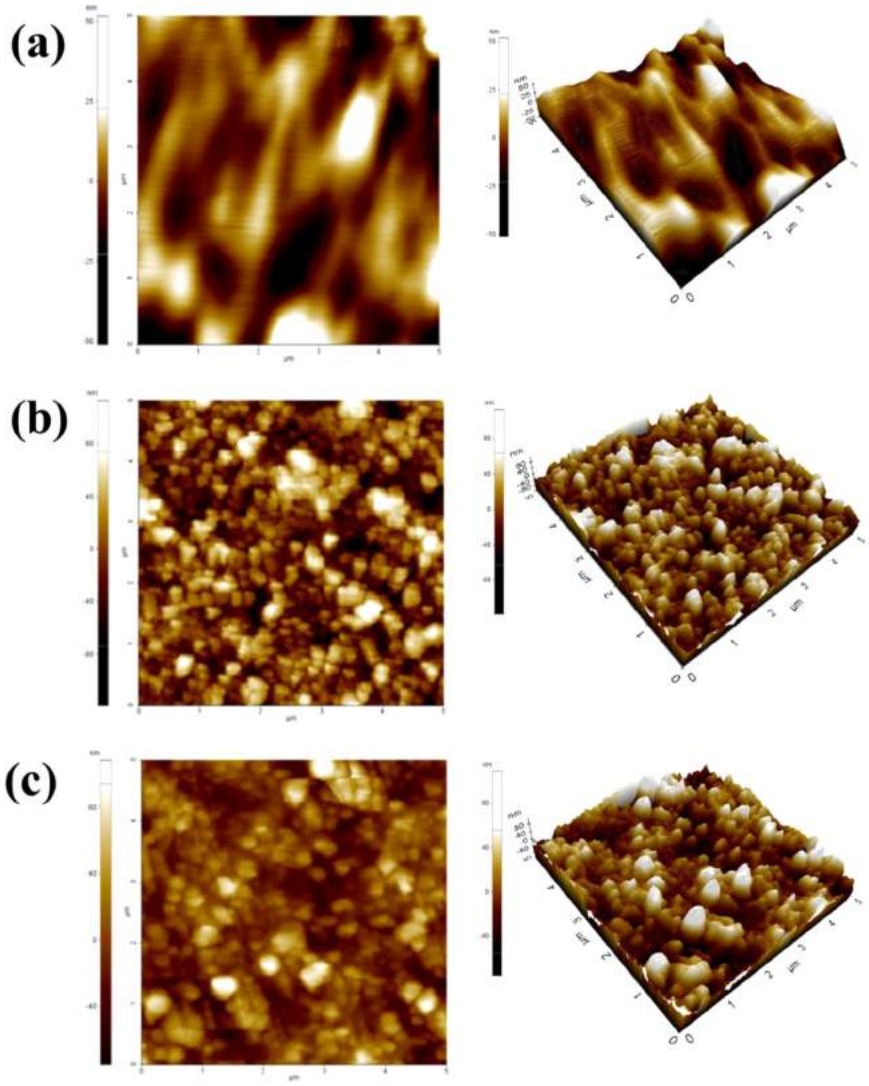

Fig. A1. AFM images of the outer surface of (a) PVDF substrate, (b) m-PVDF membrane support, and (c) CA-m-PVDF composite hollow fiber membrane.

References

[1] A. Gabelman, Hollow fiber membrane contactors, J. Membr. Sci. 159 (1999) 61.
[2] Y. Zhang, R. Wang, Gas–liquid membrane contactors for acid gas removal: recent advances and future challenges, Curr. Opin. Chem. Eng. 2 (2013) 255–262.
[3] H.-Y. Zhang, R. Wang, D.T. Liang, J.H. Tay, Modeling and experimental study of CO_2 absorption in a hollow fiber membrane contactor, J. Membr. Sci. 279 (2006) 301–310.
[4] R. Faiz, M. Fallanza, S. Boributh, R. Jiraratananon, I. Ortiz, K. Li, Long term stability of PTFE and PVDF membrane contactors in the application of propylene/propane separation using $AgNO_3$ solution, Chem. Eng. Sci. 94 (2013) 108–119.
[5] S. Atchariyawut, R. Jiraratananon, R. Wang, Separation of CO_2 from CH_4 by using gas–liquid membrane contacting process, J. Membr. Sci. 304 (2007) 163–172.
[6] R. Wang, H.Y. Zhang, P.H.M. Feron, D.T. Liang, Influence of membrane wetting on CO_2 capture in microporous hollow fiber membrane contactors, Sep. Purif. Technol. 46 (2005) 33–40.
[7] S. Mosadegh-Sedghi, D. Rodrigue, J. Brisson, M.C. Iliuta, Wetting phenomenon in membrane contactors–causes and prevention, J. Membr. Sci. 452 (2014) 332–353.
[8] I. Aouini, A. Ledoux, L. Estel, S. Mary, J. Grimaud, B. Valognes, Study of carbon dioxide capture from industrial incinerator flue gas on a laboratory scale pilot, Energy Procedia 4 (2011) 1729–1736.
[9] H. Kierzkowska-Pawlak, Carbon dioxide removal from flue gases by absorption/desorption in aqueous diethanolamine solutions, J. Air Waste Manag. Assoc. 60 (2010) 925–931.
[10] J. Hou, G. Dong, B. Xiao, C. Malassigne, V. Chen, Preparation of titania based biocatalytic nanoparticles and membranes for CO_2 conversion, J. Mater. Chem. A 3 (2015) 3332–3342.
[11] J.K.J. Yong, G.W. Stevens, F. Caruso, S.E. Kentish, In situ layer–by–layer assembled carbonic anhydrase–coated hollow fiber membrane contactor for rapid CO_2 absorption, J. Membr. Sci. 514 (2016) 556–565.
[12] J.Y. Liang, W.N. Lipscomb, Hydration of carbon dioxide by carbonic anhydrase: internal protein transfer of zinc(2+)–bound bicarbonate, Biochemistry 26 (1987) 5293–5301.
[13] R.G. Khalifah, The carbon dioxide hydration activity of carbonic anhydrase. I. Stop–flow kinetic studies on the native human isoenzymes B and C, J. Biol. Chem. 246 (1971) 2561–2573.
[14] Y. Fu, Y.B. Jiang, D. Dunphy, H. Xiong, E. Coker, S. Chou, H. Zhang, J.M. Vanegas, J.G. Croissant, J.L. Cecchi, S.B. Rempe, C.J. Brinker, Ultra–thin enzymatic liquid membrane for CO_2 separation and capture, Nat. Commun. 9 (2018) 990.
[15] J.K.J. Yong, G.W. Stevens, F. Caruso, S.E. Kentish, The use of carbonic anhydrase to accelerate carbon dioxide capture processes, J. Chem. Technol. Biotechnol. 90 (2015) 3–10.
[16] I. Iliuta, M.C. Iliuta, Investigation of CO_2 removal by immobilized carbonic anhydrase enzyme in a hollow–fiber membrane bioreactor, AIChE J. 63 (2017) 2996–3007.
[17] G. Hu, K.H. Smith, N.J. Nicholas, J. Yong, S.E. Kentish, G.W. Stevens, Enzymatic carbon dioxide capture using a thermally stable carbonic anhydrase as a promoter in potassium carbonate solvents, Chem. Eng. J. 307 (2017) 49–55.
[18] A.H.A. Al-Dhrub, S. Sahin, I. Ozmen, E. Tunca, M. Bulbul, Immobilization and

characterization of human carbonic anhydrase I on amine functionalized magnetic nanoparticles, Process Biochem. 57 (2017) 95–104.
[19] X. Fei, S. Chen, D. Liu, C. Huang, Y. Zhang, Comparison of amino and epoxy functionalized SBA–15 used for carbonic anhydrase immobilization, J. Biosci. Bioeng. 122 (2016) 314–321.
[20] B. Lv, Z. Yang, F. Pan, Z. Zhou, G. Jing, Immobilization of carbonic anhydrase on carboxyl–functionalized ferroferric oxide for CO_2 capture, Int. J. Biol. Macromol. 79 (2015) 719–725.
[21] G. Jing, F. Pan, B. Lv, Z. Zhou, Immobilization of carbonic anhydrase on epoxy–functionalized magnetic polymer microspheres for CO_2 capture, Process Biochem. 50 (2015) 2234–2241.
[22] S. Li, J. Luo, Y. Wan, Regenerable biocatalytic nanofiltration membrane for aquatic micropollutants removal, J. Membr. Sci. 549 (2018) 120–128.
[23] Y.-T. Zhang, L. Zhang, H.-L. Chen, H.-M. Zhang, Selective separation of low concentration CO_2 using hydrogel immobilized CA enzyme based hollow fiber membrane reactors, Chem. Eng. Sci. 65 (2010) 3199–3207.
[24] S.D. Minteer, Enzyme Stabilization And Immobilization–methods And Protocols, second edition, Springer, New York, 2017.
[25] U. Hanefeld, L. Gardossi, E. Magner, Understanding enzyme immobilisation, Chem. Soc. Rev. 38 (2009) 453–468.
[26] J. Hou, M.Y. Zulkifli, M. Mohammad, Y. Zhang, A. Razmjou, V. Chen, Biocatalytic gas–liquid membrane contactors for CO_2 hydration with immobilized carbonic anhydrase, J. Membr. Sci. 520 (2016) 303–313.
[27] J.K. Yong, J. Cui, K.L. Cho, G.W. Stevens, F. Caruso, S.E. Kentish, Surface engineering of polypropylene membranes with carbonic anhydrase–loaded mesoporous silica nanoparticles for improved carbon dioxide hydration, Langmuir 31 (2015) 6211–6219.
[28] J.K.J. Yong, G.W. Stevens, F. Caruso, S.E. Kentish, The resilience of carbonic anhydrase enzyme for membrane–based carbon capture applications, Int. J. Greenh. Gas Control 62 (2017) 122–129.
[29] N.G.P. Chew, S. Zhao, C. Malde, R. Wang, Superoleophobic surface modification for robust membrane distillation performance, J. Membr. Sci. 541 (2017) 162–173.
[30] H.C. Yang, Y. Xie, J. Hou, A.K. Cheetham, V. Chen, S.B. Darling, Janus membranes: creating asymmetry for energy efficiency, Adv. Mater. (2018) e1801495.
[31] N.G.P. Chew, S. Zhao, C.H. Loh, N. Permogorov, R. Wang, Surfactant effects on water recovery from produced water via direct-contact membrane distillation, J. Membr. Sci. 528 (2017) 126–134.
[32] J.-L. Li, B.-H. Chen, Review of CO_2 absorption using chemical solvents in hollow fiber membrane contactors, Sep. Purif. Technol. 41 (2005) 109–122.
[33] H.-C. Yang, W. Zhong, J. Hou, V. Chen, Z.-K. Xu, Janus hollow fiber membrane with a mussel–inspired coating on the lumen surface for direct contact membrane distillation, J. Membr. Sci. 523 (2017) 1–7.
[34] A. Liese, L. Hilterhaus, Evaluation of immobilized enzymes for industrial applications, Chem. Soc. Rev. 42 (2013) 6236–6249.
[35] X. Yang, R. Wang, L. Shi, A.G. Fane, M. Debowski, Performance improvement of PVDF hollow fiber–based membrane distillation process, J. Membr. Sci. 369 (2011) 437–447.
[36] N.G.P. Chew, S. Zhao, C. Malde, R. Wang, Polyvinylidene fluoride membrane modification via oxidant-induced dopamine polymerization for sustainable direct-contact membrane distillation, J. Membr. Sci. 563 (2018) 31–42.
[37] H.J. Hilderson, G.B. Ralston, Subcellular Biochemistry: Physicochemical Methods in the Study of Biomembranes 23 Springer Science & Business Media, USA, 2013.
[38] D.B. Knorr Jr., N.T. Tran, K.J. Gaskell, J.A. Orlicki, J.C. Woicik, C. Jaye, D.A. Fischer, J.L. Lenhart, Synthesis and characterization of aminopropyltriethoxysilane–polydopamine coatings, Langmuir 32 (2016) 4370–4381.
[39] E. Herlinger, R.F. Jameson, W. Linert, Spontaneous autoxidation of dopamine, J. Chem. Soc. Perkin Trans. 2 (2) (1995) 259–263.
[40] N.F. Della Vecchia, R. Avolio, M. Alfè, M.E. Errico, A. Napolitano, M. d'Ischia, Building–block diversity in polydopamine underpins a multifunctional eumelanin–type platform tunable through a quinone control point, Adv. Funct. Mater. 23 (2013) 1331–1340.
[41] R. Zhang, Y. Su, X. Zhao, Y. Li, J. Zhao, Z. Jiang, A novel positively charged composite nanofiltration membrane prepared by bio–inspired adhesion of polydopamine and surface grafting of poly(ethylene imine), J. Membr. Sci. 470 (2014) 9–17.
[42] J. Hou, G. Dong, Y. Ye, V. Chen, Laccase immobilization on titania nanoparticles and titania–functionalized membranes, J. Membr. Sci. 452 (2014) 229–240.
[43] K. Ragnitz, C. Syldatk, M. Pietzsch, Optimization of the immobilization parameters and operational stability of immobilized hydantoinase and l–N–carbamoylase from arthrobacter aurescens for the production of optically pure l-amino acids, Enzym. Microb. Technol. 28 (2001) 713–720.
[44] M. Carević, M. Ćorović, M. Mihailović, K. Banjanac, A. Milisavljević, D. Veličković, D. Bezbradica, Galacto–oligosaccharide synthesis using chemically modified β-galactosidase from Aspergillus oryzae immobilised onto macroporous amino resin, Int. Dairy J. 54 (2016) 50–57.
[45] C. Ji, L.N. Nguyen, J. Hou, F.I. Hai, V. Chen, Direct immobilization of laccase on titania nanoparticles from crude enzyme extracts of P. ostreatus culture for micro–pollutant degradation, Sep. Purif. Technol. 178 (2017) 215–223.
[46] Y. Liu, Y. Fang, X. Liu, X. Wang, B. Yang, Mussel–inspired modification of carbon fiber via polyethyleneimine/polydopamine co–deposition for the improved interfacial adhesion, Compos. Sci. Technol. 151 (2017) 164–173.
[47] Y. Xu, Y. Lin, M. Lee, C. Malde, R. Wang, Development of low mass–transfer–resistance fluorinated TiO_2–SiO_2/PVDF composite hollow fiber membrane used for biogas upgrading in gas–liquid membrane contactor, J. Membr. Sci. 552 (2018) 253–264.
[48] F. Lopez-Gallego, L. Betancor, C. Mateo, A. Hidalgo, N. Alonso-Morales, G. Dellamora-Ortiz, J.M. Guisan, R. Fernandez-Lafuente, Enzyme stabilization by glutaraldehyde crosslinking of adsorbed proteins on aminated supports, J. Biotechnol. 119 (2005) 70–75.
[49] J.J. Virgen-Ortíz, S. Peirce, V.G. Tacias-Pascacio, V. Cortes-Corberan, A. Marzocchella, M.E. Russo, R. Fernandez-Lafuente, Reuse of anion exchangers as supports for enzyme immobilization: reinforcement of the enzyme–support multi-interaction after enzyme inactivation, Process Biochem. 51 (2016) 1391–1396.
[50] H.P. Khameneh, T.G. Bolouri, F. Nemati, F. Rezvani, F. Attar, A.A. Saboury, M. Falahati, A spectroscopic study on the absorption of carbonic anhydrase onto the nanoporous silica nanoparticle, Int J. Biol. Macromol. 99 (2017) 739–745.
[51] F. Bougie, I. Iliuta, M.C. Iliuta, Absorption of CO_2 by AHPD–Pz aqueous blend in PTFE hollow fiber membrane contactors, Sep. Purif. Technol. 138 (2014) 84–91.
[52] R. Naim, A.F. Ismail, Effect of fiber packing density on physical CO_2 absorption performance in gas–liquid membrane contactor, Sep. Purif. Technol. 115 (2013) 152–157.
[53] S. Wongchitphimon, R. Wang, R. Jiraratananon, Surface modification of polyvinylidene fluoride–co–hexafluoropropylene (PVDF–HFP) hollow fiber membrane for membrane gas absorption, J. Membr. Sci. 381 (2011) 183–191.
[54] Y. Zhang, R. Wang, Fabrication of novel polyetherimide–fluorinated silica organic–inorganic composite hollow fiber membranes intended for membrane contactor application, J. Membr. Sci. 443 (2013) 170–180.
[55] Y. Zhang, R. Wang, L. Zhang, A.G. Fane, Novel single–step hydrophobic modification of polymeric hollow fiber membranes containing imide groups: its potential for membrane contactor application, Sep. Purif. Technol. 101 (2012) 76–84.
[56] A. Mansourizadeh, A.F. Ismail, Effect of additives on the structure and performance of polysulfone hollow fiber membranes for CO_2 absorption, J. Membr. Sci. 348 (2010) 260–267.
[57] X. Yu, L. An, J. Yang, S.-T. Tu, J. Yan, CO_2 capture using a superhydrophobic ceramic membrane contactor, J. Membr. Sci. 496 (2015) 1–12.
[58] Y. Lin, Y. Xu, C.H. Loh, R. Wang, Development of robust fluorinated TiO_2/PVDF composite hollow fiber membrane for CO_2 capture in gas-liquid membrane contactor, Appl. Surf. Sci. 436 (2018) 670–681.